

Supplemental material

Qian et al., <https://doi.org/10.1084/jem.20182100>

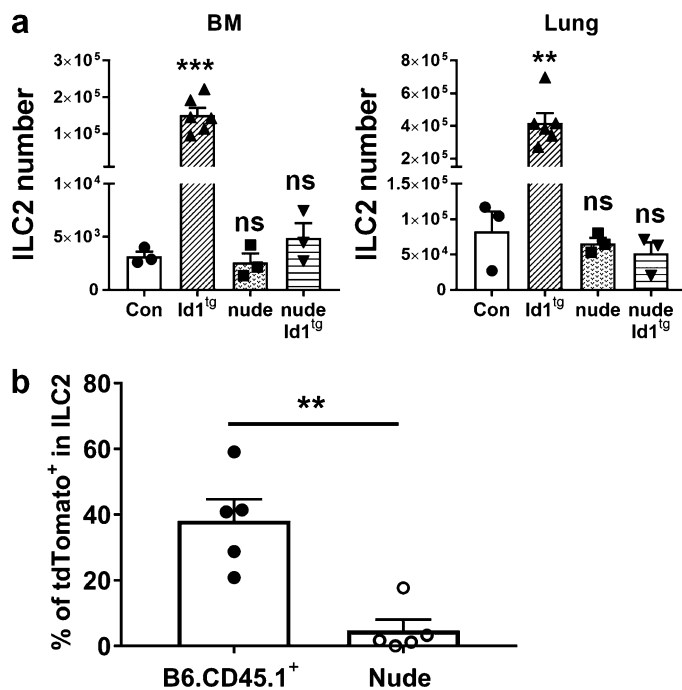


Figure S1. Thymus-dependent ILC2 production. **(a)** Athymic nude *Id1* transgenic mice do not increase ILC2 production. B6 (SJL)-Foxn1^{nug-2j}; GsrJ athymic mice were crossed with *plck*-*Id1* transgenic mice to generate nude *Id1*^{tg} mice. ILC2 ($\text{Lin}^-\text{Thy1.2}^+\text{ST2}^+$) cells were analyzed from littermates, Foxn1^{+/nu} control (Con), Foxn1^{+/nu}; *Id1*^{tg} (*Id1*^{tg}), Foxn1^{nug/nu} (nude), and Foxn1^{nug/nu}; *Id1*^{tg} (nude *Id1*^{tg}) mice. Bar graph shows total ILC2 numbers from BM and lung. Data shown are pooled from three independent experiments ($n = 3-6$). One-way ANOVA analysis was used to determine statistical significance between each mutant group and controls. Error bars are SEM. **, $P < 0.01$; ***, $P < 0.001$; ns, not significant. **(b)** Thymus-dependent production of tdTomato⁺ cells. Lethally irradiated B6. CD45.1⁺ and B6.nude mice ($n = 5$ per group) were transplanted with 100,000 $\text{Lin}^-\text{Thy1.2}^-\text{CD45.2}^+\text{TdTomato}^-$ progenitors from *plck*-cre; ROSA26-Stop-TdTomato mice. The blood of the recipients was analyzed 10–12 wk later. The gating strategy is as shown in Fig. 1 a. Data shown are the percentages of tdTomato⁺ in ILC2s ($\text{Lin}^-\text{Thy1.2}^+\text{ST2}^+$). Student's *t* tests were used to determine the statistical significance. Error bars are SEM. **, $P < 0.01$.

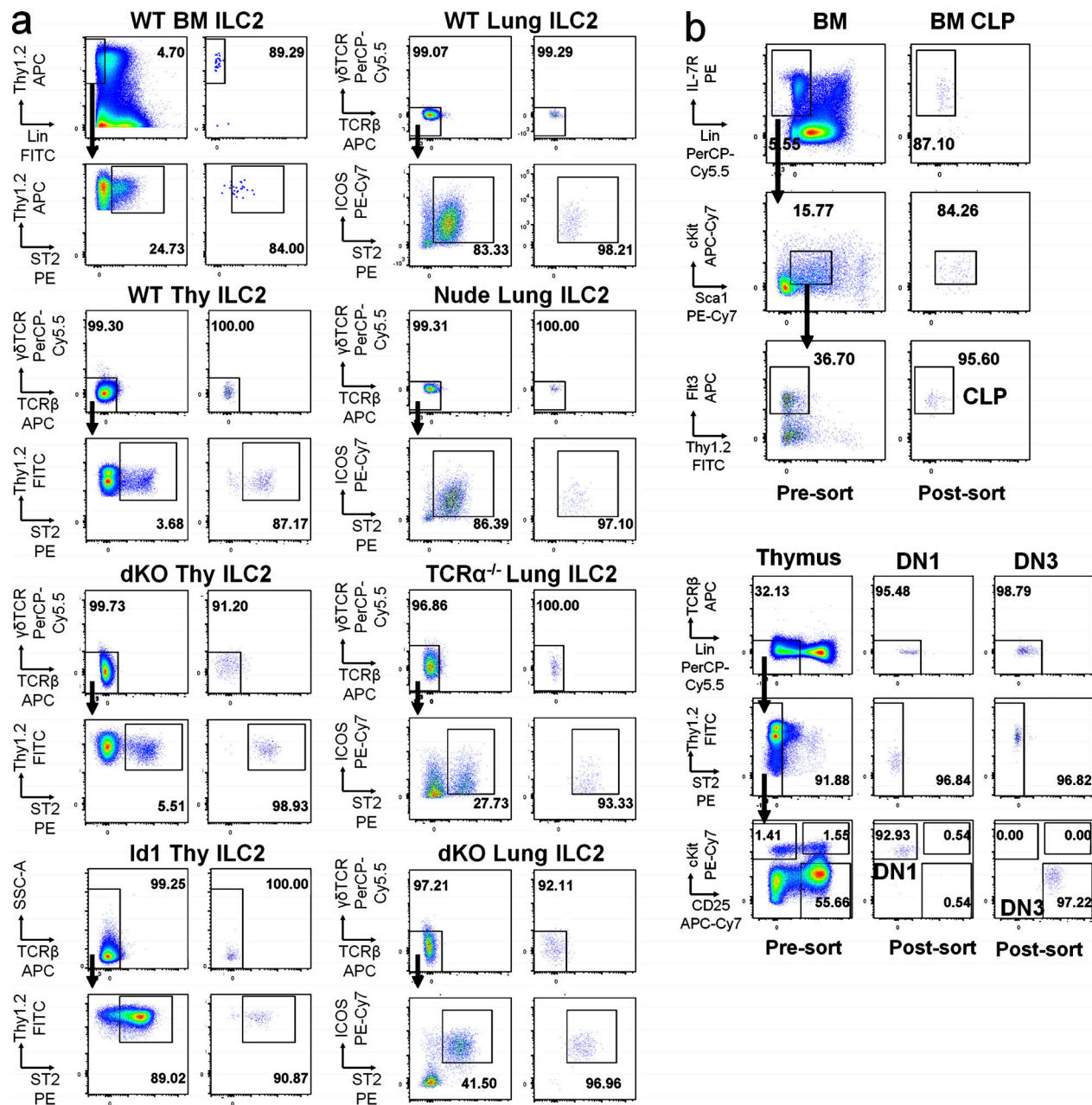


Figure S2. Post-sort analyses. **(a)** Samples used for rearrangement analyses. ILC2s from different organs were sorted from pooled preparations of multiple mice ($n = 3-12$). WT samples underwent lineage depletion before staining. Live CD45 $^+$ Lin $^-$ Thy1.2 $^+$ cells (plot not depicted) were further gated to exclude any TCR-positive cells identified by antibodies conjugated with indicated fluorophores and then scored for ST2 or ST2 and ICOS expression for ILC2s as shown by arrows. Percentages of cells in gates are listed. The pre- and post-sort profiles of each sample are as labeled. Representative graphs from at least three experiments of each genotype are shown. **(b)** Progenitors used in differentiation cultures. Lineage-depleted BM cells (top) and thymocytes (bottom) were stained with indicated antibodies and sorted for desired progenitors. Live CD45 $^+$ cells were gated in the sequence indicated by the arrows. The purity of the specified populations is shown. Data shown are representative graphs of at least six experiments.

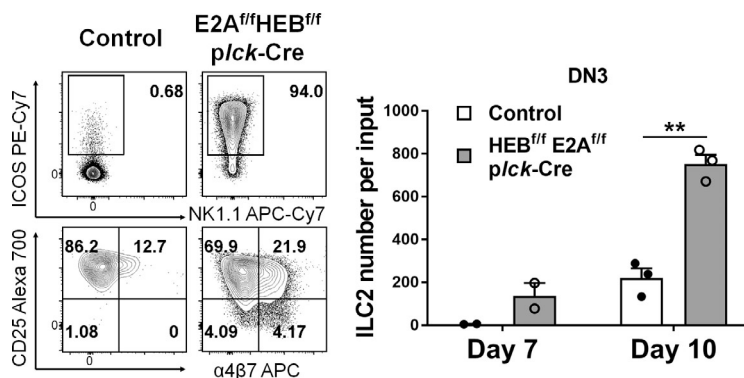


Figure S3. Ablation of E proteins at DN3 stage promotes ILC2 differentiation. DN3 cells from control and *p/cck-Cre*; E2A^{f/f}, HEB^{f/f} mice were sorted and cocultured as described in Fig. 4. Representative gating strategies of live CD45⁺TCR β - γ TCR $^{-}$ cells for defining ILC2s on day 7 are shown at the left. Numbers of ILC2s per input on days 7 and 10 were quantified ($n = 2$ or 3) at the right. Data shown are representatives of four independent experiments. Student's *t* test was used to determine statistical significance. Error bars are SEM. **, $P < 0.01$.

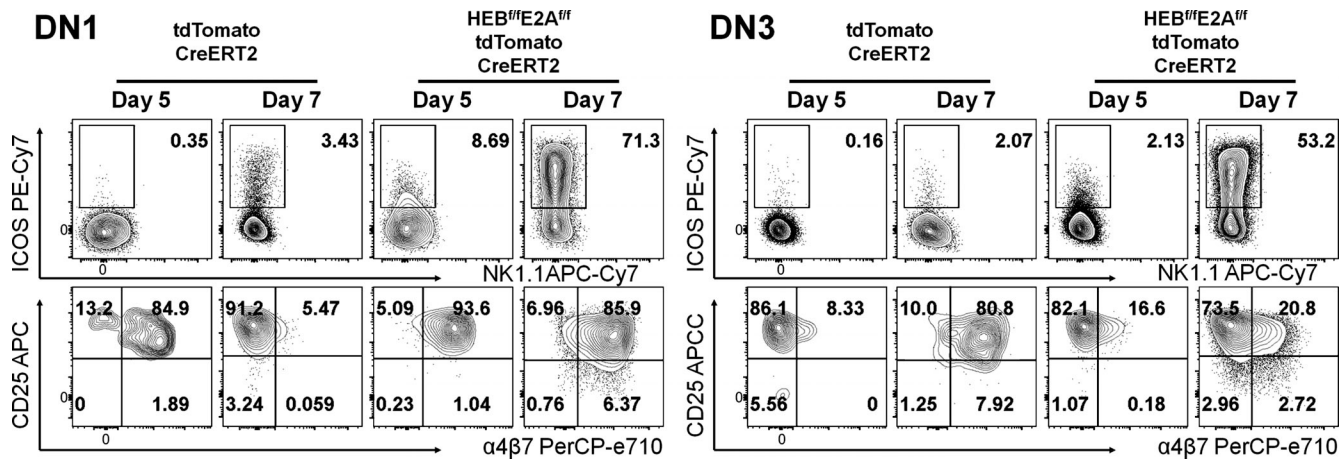


Figure S4. ILC2 differentiation profiles of the cells used for RNA-seq. Flow cytometry profiles of day 5 and 7 cells used for RNA-seq analysis shown in Fig. 6. Live CD45⁺tdTomato⁺TCR β - γ TCR $^{-}$ cells were analyzed for the expression of ICOS, NK1.1, CD25, and α 4 β 7 as described in Fig. 4.

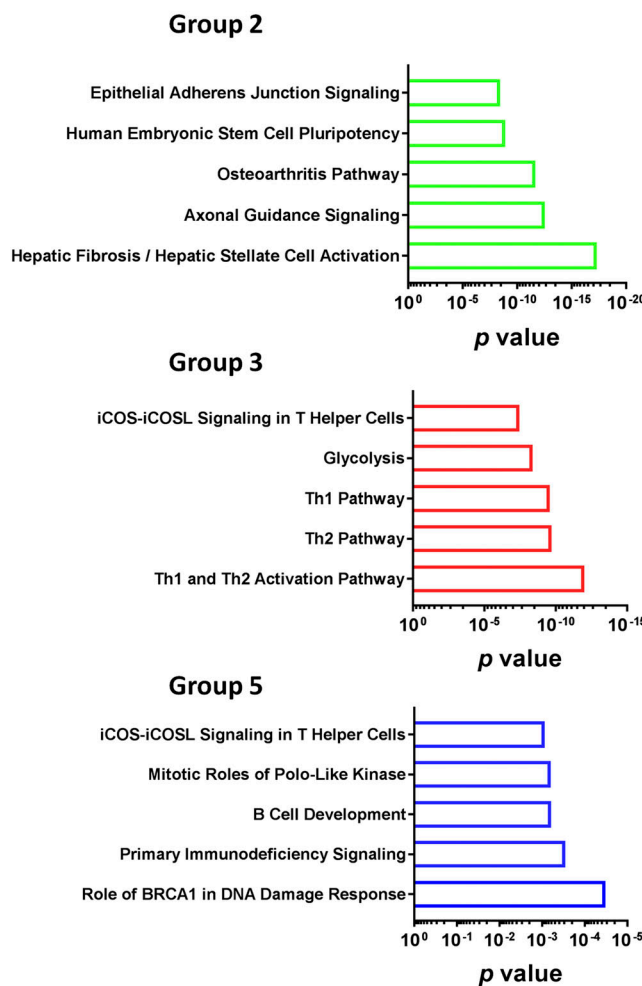
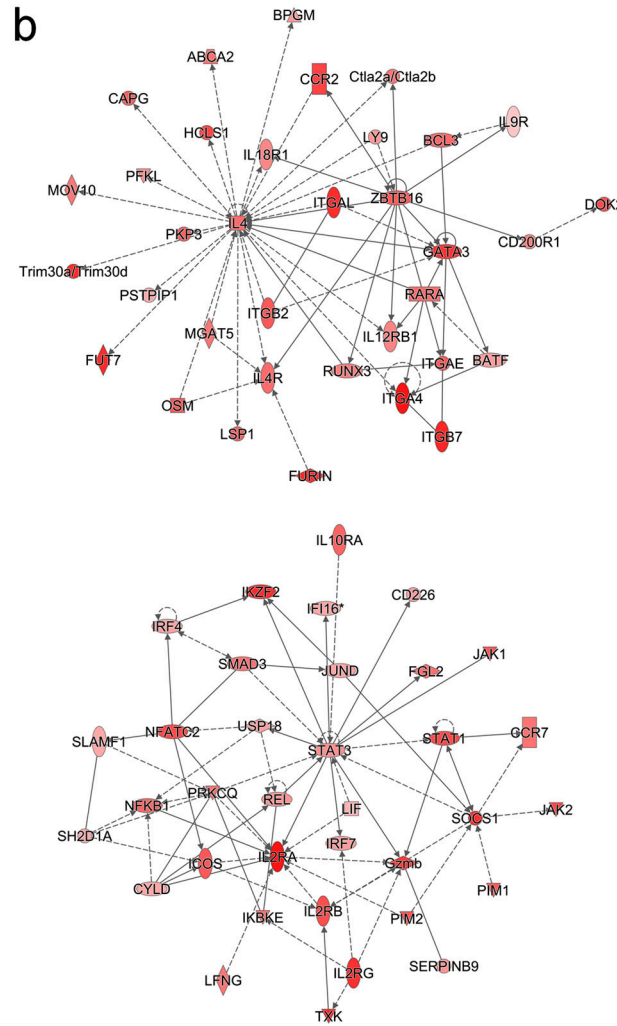
a**b**

Figure S5. Pathway analyses of genes whose expression is dramatically altered during the course of ILC2 differentiation in vitro. (a) Top five canonical pathways identified using IPA for genes of groups 2, 3, and 5 in Fig. 7 c. (b) Regulatory networks generated using IPA of group 3 genes.